HHS Public Access

Author manuscript

Nature. Author manuscript; available in PMC 2011 October 14.

Published in final edited form as:

Nature. 2011 April 14; 472(7342): 221–225. doi:10.1038/nature09879.

Recapitulation of premature aging with iPSCs from Hutchinson-Gilford progeria syndrome

Guang-Hui Liu[1], **Basam Z. Barkho**[1], **Sergio Ruiz**[1], **Dinh Diep**[3], **Jing Qu**[1], **Sheng-Lian Yang**[1], **Athanasia D. Panopoulos**[1], **Keiichiro Suzuki**[1], **Leo Kurian**[1], **Christopher Walsh**[1], **James Thompson**[4], **Stephanie Boue**[2], **Ho Lim Fung**[3], **Ignacio Sancho-Martinez**[1], **Kun Zhang**[3], **John Yates III**[4], and **Juan Carlos Izpisua Belmonte**[1,2,*]

[1]Gene Expression Laboratory, Salk Institute for Biological Studies, 10010 North Torrey Pines Road, La Jolla, California 92037, USA

[2]Center for Regenerative Medicine in Barcelona, Dr. Aiguader 88, 08003 Barcelona, Spain

[3]Department of Bioengineering, University of California at San Diego, La Jolla, California 92093, USA

[4]Department of Cell Biology, Scripps Research Institute, La Jolla, California 92037, USA

Hutchinson-Gilford progeria syndrome (HGPS) is a rare and fatal human premature aging disease[1–5], characterized by premature arteriosclerosis and degeneration of vascular smooth muscle cells (SMCs)[6–8]. HGPS is caused by a single-point mutation in the *LMNA* gene, resulting in the generation of progerin, a truncated splicing mutant of lamin A. Accumulation of progerin leads to various aging-associated nuclear defects including disorganization of nuclear lamina and loss of heterochromatin[9–12]. Here, we report the generation of induced pluripotent stem cells (iPSCs) from fibroblasts obtained from patients with HGPS. HGPS-iPSCs show absence of progerin, and more importantly, lack the nuclear envelope and epigenetic alterations normally associated with premature aging. Upon differentiation of HGPS-iPSCs, progerin and its aging-associated phenotypic consequences are restored. Specifically, directed differentiation of HGPS-iPSCs to SMCs leads to the appearance of premature senescence phenotypes associated with vascular aging. Additionally, our studies identify DNA-dependent protein kinase catalytic subunit (DNAPKcs) as a downstream target of progerin. The absence of nuclear DNAPK holoenzyme correlates with premature as well as physiological aging. Since progerin also accumulates during physiological aging[6,12,13], our results provide an *in vitro* iPSC-based model to study the pathogenesis of human premature and physiological vascular aging.

*Corresponding Author: Juan Carlos Izpisua Belmonte, belmonte@salk.edu, izpisua@cmrb.eu.

Author contributions G.H.L. and J.C.I.B. conceived the experiments; G.H.L., B.Z.B., S.R., D.D., J.Q., S.L.Y., A.D.P., K.S., L.K., C.W., J.T., and H.L.F. performed the experiments and analyzed the data; S.B., I.S.M., K.Z., and J.Y. and J.C.I.B. analyzed the data; G.H.L., S.R., B.Z.B., A.D.P., K.Z., and J.C.I.B. wrote the manuscript.

Author Information Microarray data have been deposited in NCBI-GEO under the accession number GSE24487. Reprints and permissions information is available at www.nature.com/reprints. The authors declare they have funding from Sanofi-Aventis.

Supplementary Information is linked to the online version of the paper at www.nature.com/nature.

Three HGPS primary fibroblast lines, originally isolated from patients with the classical *LMNA* mutation (Gly608Gly), were transduced with retroviruses encoding OCT4, SOX2, KLF4, c-MYC, and GFP. Nanog-positive colonies were effectively obtained when using early passage, but not late passage (>25), HGPS fibroblasts (Fig. S1a). We focused on iPSC lines of a well characterized HGPS fibroblast line, AG01972[9–12]. Compared to normal fibroblasts, HGPS fibroblasts (AG01972) showed abnormal nuclear morphology, reduced expression of the lamina components lamin B1 and LAP2β, loss of heterochromatin markers H3K9Me3, HP1α, and HDAC1, and reduced expression of nuclear proliferation marker Ki67 (Fig. 1a, S2). From HGPS fibroblasts, we derived six iPSC lines. In addition, we generated control iPSC lines from wild type fibroblasts (BJ and IMR-90 cell lines). Control and HGPS iPSC lines demonstrated pluripotent gene expression, demethylation of the OCT4 promoter and transgene silencing (Fig. 1b, S1, S3, S4a, and data not shown). They were maintained for more than 50 passages without a loss of pluripotency or the acquisition of detectable morphological or growth abnormalities. The pluripotency of each iPSC line was assessed by differentiation into the three embryonic germ layers *in vitro*, using embryoid body (EB) formation, and/or *in vivo*, by teratoma formation (Fig. S5a–d). Out of these lines, we primarily focused on HGPS-iPSC#4 and BJ-iPSC#3 for our studies (hereafter referred to as HGPS-iPSC or BJ-iPSC). Both BJ-iPSCs and HGPS-iPSCs were able to differentiate towards specialized mesoderm-derivatives such as smooth muscle cells (SMC), endothelial cells (Fig. S6a), or beating cardiomyocytes (Movie S1–S2). Moreover, all analyzed iPSC lines showed normal chromosomal integrity (Fig. S5e). Finally, *LMNA* sequencing confirmed the presence of the classical mutation in HGPS-iPSCs (Fig. S5f). Altogether, these data indicate that the somatic cells from HGPS patients, despite their significant premature senescence phenotypes and nuclear defects, have been properly reprogrammed and can be effectively maintained in a pluripotent state.

Lamin A/C protein is expressed in differentiated somatic cells but is absent in embryonic stem cells (ESCs)[11,14]. Therefore, we next examined the expression of lamin A/C in the generated iPSC lines. As shown in Fig 2a, lamin A/C expression is significantly downregulated in iPSCs, compared to their parental fibroblasts, whereas lamin B1 transcripts were upregulated. Although progerin should follow a similar pattern of expression as observed for lamin A/C, *LMNA* expression is independent of promoter methylation status (Fig. S4b)[15]. Indeed, a complete loss of progerin mRNA in HGPS-iPSCs was observed (Fig. 2a). Furthermore, expression of lamin A/C and progerin proteins was practically undetectable (Fig. 2b, S4c).

Since HGPS-iPSCs did not express progerin, we examined whether the nuclear abnormalities observed in HGPS fibroblasts would also be absent at the pluripotent stage. Our results indicate that all of the epigenetic, nuclear lamina and proliferation parameters analyzed in HGPS-iPSCs were indistinguishable from BJ-iPSCs (Fig. 2b–c, S3, S7). In addition, the nuclei of HGPS-iPSCs displayed the characteristic wrinkles and lobes observed in hESCs and iPSCs (Fig. S8), indicative of a reprogramming of the nuclear envelope components. Since the nuclear envelope associates with and regulates heterochromatin[11,16], we next examined genome-wide CpG methylation in HGPS fibroblasts, BJ fibroblasts, HGPS-iPSCs, BJ-iPSCs, and H9 hESCs. Using bisulfite padlock probes and Illumina

sequencing, we captured and quantified the methylation level of an average of 95,932 CpG sites within a set of 16,206 well annotated Differentially Methylated Regions (DMRs)[17] per cell line (Table S1). The correlation coefficient of the global methylation levels between the pluripotent lines (BJ-iPSCs, HGPS-iPSCs and H9 hESCs) and the corresponding fibroblasts indicated that the generated pluripotent lines are much more closely related to each other and to hESCs than the two fibroblast lines (Fig. 2d). Interestingly, 586 autosome genes were found to be associated with regions that exhibited methylation differences between HGPS and BJ fibroblasts (Table S2, Fig S9a). Furthermore, based on DAVID[18,19] analysis, we found that these genes were enriched for 21 Gene Ontology terms, most of which were related to development and transcriptional regulation (Fig S9a). In contrast, methylation differences between HGPS-iPSCs and BJ-iPSCs were only found for 33 autosome genes (Table S3), which showed no significant functional enrichment. Therefore, the presence of progerin in HGPS fibroblasts appears to lead to major epigenomic changes in various pathways. These changes were no longer present in HGPS-iPSCs, coinciding with the downregulation of progerin. Finally, genome-wide mRNA profiling demonstrated that HGPS-iPSCs and BJ-iPSCs are closely related together with H9 hESCs, and discrete from their parental fibroblasts (Fig. S9b–d). These results demonstrate the complete resetting of the nuclear architecture, epigenome and global gene expression in HGPS cells after being reprogrammed to pluripotency.

To test whether the expression of progerin could be re-activated, we first subjected HGPS-iPSCs to *in vitro* differentiation via EB formation. Progerin mRNA was selectively induced in differentiated HGPS-iPSCs, but not in differentiated BJ-iPSCs (Fig. S10a). In contrast, lamin A was upregulated in both HGPS-iPSCs and BJ-iPSCs (Fig. S10a). This reversible suppression of progerin expression by reprogramming, and subsequent reactivation upon differentiation, provides a unique model system to study human premature aging pathologies. Progerin is known to accumulate mainly in arterial SMCs of HGPS patients, and vascular SMC degeneration is one of the characteristics of HGPS-associated arteriosclerosis[6,7,20]. In fact, vascular SMC senescence has been involved in the advanced arteriosclerosis of normal populations[7,21,22]. We therefore next asked whether SMCs differentiated from HGPS-iPSCs exhibit premature senescence phenotypes. Using a directed differentiation protocol, we obtained SMC populations from HGPS-iPSCs and BJ-iPSCs, the majority of which expressed characteristic SMC markers such as smooth muscle actin (SMA) and calponin (Fig. S6a). Immunoblotting and RT-PCR analyses confirmed the expression of progerin in HGPS-iPSC, but not BJ-iPSC-derived SMCs (hereafter referred to as “HGPS-SMC” and “BJ-SMC”, Fig. S6b–c). To model SMC senescence *in vitro*, the differentiated SMCs were serially passaged in culture. As shown in Fig. 3a–c and S10b, an increasing frequency of misshapen nuclei and a loss of the heterochromatin mark H3K9Me3 were specifically observed in HGPS-SMCs after serial passaging. HGPS-SMCs at later passages (i.e. passage 5) showed the typical characteristics of premature senescence, including increased senescence-associated-β-Gal (SA-β-Gal) staining (Fig. 3d–e, S10c), reduced telomere length (Fig. 3f), reduced number of Ki67-positive cells (Fig. 3g, S10d), and compromised cell proliferation (Fig. 3h, S10e). We also found a selective upregulation of senescence-related transcripts in HGPS-SMCs (Fig. S10f). To test whether the observed HGPS-related cell phenotypes were specific to SMCs, we differentiated HGPS-iPSCs into

fibroblasts and measured progerin-associated parameters. Progerin expression in HGPS-iPSC-derived fibroblasts was detectable as early as passage 5 (Fig. S11a). However, we were unable to detect a loss of lamina or heterochromatin markers before passage 10 (Fig. S11b–c). Nonetheless, these defects were present specifically in HGPS-iPSC-derived fibroblasts, in contrast to control iPSC-derived fibroblasts analyzed at similar passage (data not shown). Thus, even though direct comparison of SMCs and fibroblasts is not possible due to their different culture conditions, our observations demonstrate that mesoderm lineages derived from HGPS-iPSCs display a characteristic HGPS phenotype.

We next investigated whether progerin accumulation is the direct cause of the accelerated cell senescence observed in HGPS-SMCs. To this end, we induced ectopic expression of progerin in human primary vascular SMCs. We found that introduction of progerin in wild type SMCs resulted in compromised cell proliferation and nuclear defects, as we had observed in HGPS-SMCs (Fig. 3i, S12). As a complementary approach, we transduced HGPS-iPSCs with a lentiviral vector expressing a progerin-specific shRNA[23]. The modified iPSCs showed normal karyotypes as well as normal expression of lamina/epigenetic and pluripotent markers (Fig. S13a–b). After EB-based differentiation, both the mRNA and protein levels of progerin, but not those of lamin A, were substantially downregulated in the progerin-shRNA “corrected” HGPS-iPSCs compared to control cells (Fig. 3j, S13c–d). We next differentiated these “progerin-free” HGPS-iPSCs into SMCs (Fig. S14a). A dramatic improvement in the proliferation capability, as well as a downregulation of senescence-related transcripts, was found in the SMCs differentiated from the corrected HGPS-iPSCs (Fig. 3k and S14b–c). Furthermore, transduction of progerin shRNA into early passage HGPS-iPSC-derived fibroblasts resulted in a clear restoration of nuclear morphology and heterochromatin markers after extended culture (Fig. S15). Taken together, these data identify progerin as the key factor underlying the premature senescence phenotypes of HGPS-iPSC-derived cells.

Since phenotypic characteristics of premature aging were able to be recapitulated by directed differentiation of the HGPS-iPSCs, we next investigated whether this model could serve to identify novel senescence-related markers. By using a sensitive MudPIT proteomic approach[24],[25], we identified DNA-dependent protein kinase catalytic subunit (DNAPKcs) as a hitherto unknown binding partner of progerin (Table S4). DNAPK holoenzyme, comprising of DNAPKcs and its regulatory subunits Ku70/Ku80, is involved in various aging-related cellular events[26],[27], and DNAPKcs or Ku70/Ku80-deficient mice exhibit accelerated aging[27],[28]. To further confirm the association of progerin with DNAPKcs, we performed co-immunoprecipitation (co-IP) experiments. As shown in Fig 4a, ectopically expressed progerin associated tightly with endogenous DNAPKcs. In contrast, lamin A showed weak interaction with DNAPKcs, whereas both progerin and lamin A exhibited similar binding to lamin B1. Neither progerin nor lamin A co-immunoprecipitated with endogenous WRN protein. Since most of the nuclear proteins in complex with lamin A are destabilized in HGPS cells[9],[29], we analyzed the status of DNAPKcs in primary HGPS fibroblasts. We observed decreased nuclear DNAPKcs in HGPS fibroblasts when compared to normal fibroblasts (Fig. 4b–c). In addition, the regulatory subunits Ku70/Ku80 were also downregulated in HGPS fibroblasts (Fig. S16a). Interestingly, we detected a complete restoration of DNAPKcs/Ku70/Ku80 expression in HGPS-iPSCs (Fig. 4b, 4d, S3, S16b),

although a deficiency in the expression of these proteins reappeared after differentiation into SMCs (Fig. 4e). These observations suggest that the downregulation of DNAPKcs in HGPS cells is dependent on the accumulation of progerin in differentiated cells. In fact, ectopic expression of progerin in primary vascular SMCs diminished DNAPKcs/Ku80 protein expression (Fig. 4f, S17). We next tested whether inactivation of DNAPKcs could partially contribute to some of the phenotypes observed in HGPS-SMCs. We found that knockdown of DNAPKcs reduced the proliferation of primary vascular SMCs (Fig. S18a). Finally, we extended our results and found that progressive loss of DNAPKcs/Ku70/Ku80 also occurs in fibroblasts isolated from normally aging individuals (Fig. S18b). Overall, our data suggest that deficiency of the DNAPK holoenzyme may constitute a novel marker for premature as well as physiological aging.

In summary, our results not only highlight the plasticity of the lamina-epigenetics axis, but also point to the fact that the altered structure of the nuclear envelope, as well as the epigenetic modifications that accumulate during physiological aging[12] or under specific disease conditions[1],[11], can be restored to normalcy by reprogramming (Fig. S19). The gradual onset and complexity of aging has impeded progress in understanding the pathogenesis of aging-related cardiovascular disorders. Recently, striking similarities between normal aging-associated and HGPS-associated arteriosclerosis have been reported[6],[16]. Indeed, the levels of progerin increase gradually during physiological aging[6]. Our study provides the first evidence that, in a progerin-dependent manner, HGPS-iPSC-derived SMCs reach senescence-related phenotypes earlier than their normal counterparts. The iPSC-based accelerated aging model presented here and by Zhang et al[30] may provide an avenue to model and study the pathogenesis of human aging-related vascular diseases as well as various human laminopathies[1].

METHODS SUMMARY

iPSCs were generated from human fibroblasts with retroviruses encoding OCT4/SOX2/KLF4/c-MYC/GFP, and cultured on MEF feeder cells or Matrigel. SMCs were differentiated from iPSCs-derived CD34+ progenitor cells following an OP9-based protocol.

ONLINE METHODS

Cell culture

H9 hESCs (WiCell Research) and iPSCs were maintained on a layer of mitotically inactivated mouse embryonic fibroblasts (MEFs) in hESC medium: DMEM/F12 (Invitrogen) supplemented with 0.1 mM non-essential amino acids (Invitrogen), 1 mM glutamax (Invitrogen), 20% Knockout Serum Replacement (Invitrogen), 55 μM β-mercaptoethanol (Invitrogen) and 10 ng/ml bFGF (Joint Protein hESCs and iPSCs were also cultured in Matrigel (BD Biosciences) with mTeSR medium (Stem Cell Technologies). Human HGPS fibroblasts AG01972, AG11498, AG06297, and normal fibroblasts GM00038 (9 year), AG05247 (87 year), and AG09602 (92 year) were purchased from Coriell Cell Repository. BJ normal human fibroblasts (CRL-2522) were purchased from ATCC. All human fibroblasts were cultured at 37°C in DMEM containing glutamax, non-essential amino acids, sodium pyruvate, and 15% fetal bovine serum (FBS). Human aortic smooth

muscle cells were purchased from Lonza and maintained in SmGM-2 medium (Lonza, Cat. # CC-3182).

Reagents

Antibodies were obtained from the following sources. *Abcam:* anti-NANOG (ab21624), anti-H3K9Me3 (ab8898), anti-progerin (ab66587), anti-emerin (ab14208); anti-Ku70 (ab2172); *Santa Cruz Biotechnology:* anti-Oct-3/4 (sc-5279), anti-SOX2 (sc-17320), anti-HDAC1 (sc-7872), anti-DNAPKcs (sc-9051), anti-lamin A/C (sc-6215), anti-lamin A/C (sc-7293), anti-lamin B1 (sc-6217); *Cell Signaling:* anti-HP1α (2616); anti-Ku80 (2753); *R&D systems:* anti-Foxa2 (AF2400); Millipore: anti-TRA-1-60 (MAB4360) ; *Sigma:* anti-β-Tubulin III (T2200), anti-SMA(A5228), anti-Flag (M2), and anti-tubulin (T5168); *Dako:* anti-calponin (clone CALP); anti-endoglin (clone SN6h); *BD Transduction Laboratories:* anti-LAP2β (611000); *MBL*: Agarose-conjugated anti-GFP.

Plasmids

The pMXs vector containing the human cDNAs for *OCT4*, *SOX2, KLF4* and *c-MYC* were purchased from Addgene (17217, 17218, 17219 and 17220, respectively). pBABE-puro-GFP-progerin and pBABE-puro-GFP-wt-lamin A were purchased from Addgene (17663 and 17662, respectively). Flag-progerin lentiviral vector was kindly provided by Dr. Lucio Comai [31]. For the generation of the shRNA expression vectors against progerin and DNAPKcs, corresponding oligos (see Table S5) were cloned into a MluI/ClaI-cleaved pLVTHM plasmid (Addgene, 12247). All the constructs generated were subjected to DNA sequencing to confirm accurate shRNA target sequence.

Retrovirus and lentivirus production

For retrovirus production, 293T cells were transfected with the pMXs vectors carrying *OCT4*, *SOX2*, *c-MYC*, *KLF*4, or *GFP* cDNAs, together with the packaging plasmids (pCMV-gag-pol-PA and pCMV-VSVg, provided by Dr. Gerald Pao, The Salk Institute) using Lipofectamine 2000 (Invitrogen). Retroviruses were collected 36–48 h after transfection, and filtered through a 0.45 μM filter. Lentiviruses were generated by co-transfecting the pLVTHM vector together with the packaging plasmids (psPAX2 and pMD2.G, from Addgene, 12260 and 12259 respectively) into 293T cells using Lipofectamine 2000 (Invitrogen). Lentiviruses were collected 36 hours after transfection and concentrated by ultracentrifugation.

iPSCs Generation

For the generation of human iPSCs, human fibroblasts were seeded in a 6-well plate and spin-infected with a mix of high-quality retroviruses encoding OCT4, SOX2, KLF4, c-MYC, and GFP in the presence of 4 μg/ml polybrene. Three infections on consecutive days were performed. Six days after the first infection, fibroblasts were gently individualized with TrypLE (Invitrogen) and seeded onto fresh MEFs in the fibroblast culture medium. After 24 h, the medium was switched to hESC medium, and changed every 1–2 days depending on cell density. To establish the iPSC lines, colonies were manually picked and transferred onto

MEF feeder cells for several passages before being transferred to Matrigel/mTesR conditions.

Lentiviral infection of iPSCs

HGPS-iPSC#4 cell line cultured on Matrigel was treated with 10 μM ROCK inhibitor Y-27632 for 1 h and then individualized with TrypLE. Cells were infected in suspension with either the concentrated lentivirus pLVTHM or pLVTHM-shRNA-Progerin in the presence of ROCK inhibitor and polybrene (4 μg/ml) for 1 h. Cells were centrifuged to remove the lentivirus and seeded back on fresh feeder MEFs in hESC media containing ROCK inhibitor. After being cultured for a few days, small colonies were manually passaged as a pool of colonies onto fresh MEFs to establish new iPSC lines. GFP expression was used as an indicator to determine successful integration of the lentiviruses.

Cell differentiation

For embryoid bodies (EBs) based differentiation, the iPSC colonies growing on MEFs were detached with dispase treatment, resuspended in DMEM/F12 medium supplemented with 0.1 mM non-essential amino acids, 0.5 mM L-glutamine, 10% FBS (Atlanta Biologicals), and 55 μM β-mercaptoethanol and cultured in low attachment 6-well plates for 4 days. The EBs were then plated on gelatin-coated plates and maintained for another 10–17 days. Differentiation of iPSCs into fibroblasts was performed as previously described[32]. Directed differentiation toward smooth muscle cells (SMCs) was performed essentially as previously described[32] with slight modifications. Irritated OP9 cells were plated at 1×10^5 cells/well onto gelatinized 6-well plates in OP9 growth medium. After the formation of confluent iPS cell cultures for 4 and 5 days, undifferentiated iPS cells were harvested by treatment with 1 mg/mL dispase and dispersed by scraping to maintain the cells in small clumps. Concurrently, iPS cultures growing under the same conditions were used to obtain single cell suspension for counting. The iPSCs were added to OP9 cultures at a density of 3×10^5/2 mL per well of a 6-well plate in half TesR medium and half hESC media. iPSCs were allowed to recover for 1–2 days in hESC media. At day 0 of differentiation, the media was changed to Knockout DMEM supplemented with 10% FBS (HyClone), 10 mM β-mercaptoethanol, 1 mM L-glutamine, and 100 mM nonessential amino acids. The iPSC/OP9 cocultures were incubated for up to 10 days at 37°C in 5% CO2 conditions with medium change every other day. After 10 days of differentiation, the coculture cells were harvested with TrypLE (Invitrogen) for single-cell suspension and labeled with CD34 microbeads kit (Miltenyi Biotech, Cat. #130-046-702). Following the manufacturer's protocol, cells were passed through MS separation column attached to a Midi-MACS separation unit (Miltenyi Biotech) to obtain a magnet-retained fraction of purified CD34+ cells. Isolated CD34+ cells were then plated in smooth muscle cell media (SmGM-2 BulletKit, Lonza, Cat. # CC-3182) and maintained at 37°C in 5% CO2 conditions with medium change every 2–3 days[34]. SMCs were passaged using TrypLE (diluted 1:4) for 3 minutes at 37°C. To analyze early onset of senescence, cells were passaged at a ratio of 1:3 (~6000–7500 cells/cm^2) only when the cells reached confluence. To calculate population doublings, SMCs seeded at 3500 cells/cm2 were passaged once culture reached 85–90% confluence. Cell growth was measured at every passage by calculation of accumulated population doublings using the

formula (logH -logS) / log2.0 (H=number of cells harvested; S=number of cells seeded on the first day of each passage).

Protein and mRNA analysis

Cells were lysed and subjected to immunoblotting analysis according to the previously described method[35]. Total RNA was extracted using Trizol (Invitrogen) followed by cDNA synthesis using High capability RNA-to-cDNA Mater Mix (Invitrogen). Quantitative RT-PCR was performed using SYBR Green PCR Master Mix (Applied Biosystems). Primer sequences are listed in Table S5.

Immunofluorescence microscopy

Cells were fixed with 4% formaldehyde in PBS at room temperature (RT) for 20–30 min. After fixation, cells were treated with 0.4% Triton X-100 in PBS for 5 min at RT. After blocked with 10% FBS in PBS for 30 min, cells were incubated at RT for 1 h or at 4°C overnight with the primary antibody, followed by washing in PBS and incubation at RT for 1 h with the corresponding secondary antibody. Nuclei were stained with Hoechst 33342 (Invitrogen). Quantitative microscopy measurements were carried out as described previously[9]. Error bars represent standard deviations.

Immunohistochemical detection of NANOG

Cells were fixed with 4% formaldehyde in PBS at RT for 30 min, and permeabilized with 0.4% Triton-X100 in PBS for 10 min. Then the cells were incubated overnight with rabbit anti-human NANOG antibody in 1% BSA/PBS, followed by incubation with a secondary biotin-conjugated anti-rabbit antibody for 2 hours. Finally, cells were incubated with streptavidin-HRP for 1 hour (Vector), and NANOG-positive cells were visualized with a DAB substrate kit (Vector).

Teratoma analysis

To test pluripotency *in vivo*, NOD-SCID IL2Rgamma^{null} mice (Jackson laboratories) were injected with the indicated iPSC lines and teratoma formation assessed. Briefly, ~10^6 iPSCs in ~50uL of hESC medium were injected into the testis or kidney capsule of anesthetized mice. Mice were monitored for teratoma formation and euthanized ~6–12 weeks after injection. Teratomas were harvested, processed and analyzed by hematoxylin-eosin staining and immunostaining. All animal experiments were performed with approval of The Salk Institute Institutional Animal Care and Use Committee (IACUC).

Mutation validation

Primer sequences to amplify exon 11 of the *LMNA* gene are listed in Table S5. 50 μl PCR reactions using 3 ng genomic DNA templates, 100 nM of the forward and reverse primers with 25 μl Taq 2× Master Mix (NEB) was performed at 94°C for 2 min, 34 cycles of 94°C 30 s, 55.5°C for 40 s, and 72°C for 40 s, and finally 72°C for 3 min. Products were purified with 0.9× volume of AMPure beads (Agencourt). Amplicons were sequenced by capillary Sanger sequencing (Genewiz). Results were visualized using an ABI Sequence Scanner.

Genome–wide DNA methylation analysis

Genomic DNA was extracted using ALLPrep DNA/RNA Mini kit (Qiagen). Bisulfite conversion and capture reaction was carried out on each sample (genomic DNA of fibroblasts, iPSCs, or hESCs). The detailed protocol for genomic DNA methylation has been described previously[36], and the detailed information for DNA methylation is presented in Table S1.

Bisufite sequencing of OCT4 and *LMNA* promoters

Bisulfite conversion was carried out using 2 μg of purified genomic DNA using the Zymo EZ-DNA Methylation Gold Kit (Zymo Research) following the manufacturer's instructions. PCR was set up using previously published primers[15]. Cycling was terminated at 35 cycles. PCR products were purified using 2 % Size-Select E-gel (Invitrogen) and reamplified for 10 cycles using Phusion HF enzyme (NEB). PCR products were cloned using Zero-blunt PCR Cloning kit (Invitrogen) and heat transfected to TOP10 E. coli competent cells (Invitrogen). Individual colonies were selected and sent for single pass sequencing.

DNA microarray and Bioinformatics analysis

The GeneChip microarray processing was performed by the Functional Genomica Core in the Institute for Research in Biomedicine (Barcelona, Spain) according to the manufacturer's protocols (Affymetrix, Santa Clara, CA). The amplification and labeling were processed as indicated in Nugen protocol with 25ng starting RNA. For each sample, 3.75μg ssDNA were labeled and hybridized to the Affymetrix HG-U133 Plus 2.0 chips. Expression signals were scanned on an Affymetrix GeneChip Scanner (7G upgrade). The data extraction was done by the Affymetrix GCOS software v.1.4. The statistical analysis of the data was performed using ArrayStar 3. Briefly, raw CEL files were imported together with gene annotation from NetAffix (from 11/13/2009) and after checking for top replication quality for each of the 5 pairs of samples (R^2>0.99), data was summarized at the gene level (20,765 genes) and the median was used for each gene and sample type. As both H9 hESCs and HGPS-iPSCs originate from female samples, and in order to remove any possible bias introduced by the X and Y chromosome-coded genes, we performed the same analysis with only autosome genes (19,884 genes). The result of the hierarchical clustering is very similar to the one using all genes and is shown in Figure 2f. In addition, a principal component analysis was performed on RMA-normalized probeset intensity values for autosomes using the prcomp function in R (http://www.r-project.org/) (the same figure including all genes gave highly similar results, data not shown). A figure illustrating the two first principal components is shown in figure S9c. Differences between some of the samples is shown using scatter plot of RMA-normalized intensity values in figure S9b.

Multidimensional Protein Identification Technology (MudPIT) analysis of progerin-associated proteins

The immunoprecipitation for MudPIT assay was performed as previously described[24,25]. In brief, HEK293T cells were transfected with GFP-progerin or GFP and maintained in culture for 48 h. After cells were lysed, the GFP-progerin, GFP, and their associated proteins were immunoadsorbed to anti-GFP agarose. The immunoprecipitates were then eluted with 8 M

urea in 100 mM Tris, pH 8.5. The samples were reduced by adding 0.3 μL of 1M TCEP (for a final concentration of 5 mM TCEP) and incubated at RT. To alkylate, 1.2 μL of Iodoacetamide (10 mM final concentration) was added and the samples were subsequently incubated at RT in the dark for 15 minutes. The addition of 180 μL of 100 mM Tris pH 8.5 diluted the solutions to 2 M Urea. Calcium chloride (100 mM) was then added (2.4 μL) for a final concentration of 1 mM CaCl2. Trypsin (0.5 μg/μL) was added in the amount of 7.0 μL. The resulting mixtures were then shaken for 18 hours and incubated in the dark at 37 °C. To neutralize 13.5 μL of Formic Acid (90%) was added for a final concentration of 5% Formic Acid. The tubes were centrifuged for 30 minutes at 2 °C in a table-top centrifuge. Upon completion of the digestion, the proteins were pressure-loaded onto a fused silica capillary desalting column containing 3 cm of 5-μm strong cation exchange (SCX) followed by 3 cm of 5-μm C18 (reverse phase or RP material) packed into an undeactivated 250-μm i.d capillary. Using 1.5 mL of buffer A (95% water, 5% acetonitrile, and 0.1% formic acid) the desalting columns were washed overnight. Following the desalting process, a 100-μm i.d capillary consisting of a 10-μm laser pulled tip packed with 10 cm 3-μm Aqua C18 material (Phenomenex, Ventura, CA) was attached to the filter union (desalting column-filter union-analytical column) and the entire split-column (desalting column-filter union-analytical column) was placed in line with an Agilent 1100 quaternary HPLC (Palo Alto, CA) and analyzed using a modified 6-step separation, described previously[25]. The buffer solutions used were 5% acetonitrile/0.1% formic acid (buffer A), 80% acetonitrile/0.1% formic acid (buffer B), and 500 mM ammonium acetate/5% acetonitrile/0.1% formic acid (buffer C). Step 1 consisted of a 90 min gradient from 0–100% buffer B. Steps 2–5 had the following profile: 3 min of 100% buffer A, 2 min of X% buffer C, a 10 min gradient from 0–15% buffer B, and a 97 min gradient from 15–45% buffer B. The 2 min buffer C percentages (X) were 20, 40, 60, 80% respectively for the 6-step analysis. In the final step, the gradient contained: 3 min of 100% buffer A, 20 min of 100% buffer C, a 10 min gradient from 0–15% buffer B, and a 107 min gradient from 15–70% buffer B. As peptides eluted from the microcapillary column, they were electrosprayed directly into an LTQ 2-dimensional ion trap mass spectrometer (ThermoFinnigan, Palo Alto, CA) with the application of a distal 2.4 kV spray voltage. A cycle of one full-scan mass spectrum (400–1400 m/z) followed by 8 data-dependent MS/MS spectra at a 35% normalized collision energy was repeated continuously throughout each step of the multidimensional separation. Application of mass spectrometer scan functions and HPLC solvent gradients were controlled by the Xcalibur datasystem.

As each step was executed, its spectra were recorded to a RAW file. This data was then converted into .ms2 format through the use of RawXtract (Version 1.9). From the .ms2 files, poor quality spectra were removed from the dataset using an automated spectral quality assessment algorithm[37]. MS/MS spectra remaining after filtering were searched with the SEQUEST™ algorithm[38] against the NCBI RefSeq Human (04-23-2010) protein database concatenated to a decoy database in which the sequence for each entry in the original database was reversed[25],[39]. All searches were parallelized and performed on a Beowulf computer cluster consisting of 100 1.2 GHz Athlon CPUs[40]. No enzyme specificity was considered for any search. SEQUEST results were assembled and filtered using the DTASelect (version 2.0) program. DTASelect 2.0 uses a linear discriminant analysis to

dynamically set XCorr and DeltaCN thresholds for the entire dataset to achieve a user-specified false positive rate. The false positive rates are estimated by the program from the number and quality of spectral matches to the decoy database. The hits detected uniquely in the GFP-progerin sample but not in GFP sample represent proteins that are specifically associated with progerin, by either direct or indirect interactions.

Co-Immunoprecipitation

BJ human fibroblasts were transduced with retrovirus encoding GFP-progerin, GFP-lamin A or GFP, and maintained in culture for 72h. For immunoprecipitation, cells were lysed in ice-cold lysis buffer (250 mM NaCl, 0.5% Triton X-100, 50 mM Tris, pH 7.5, 1 mM EGTA, 1 mM EDTA, 10% glycerol, and complete protease inhibitor cocktail (Roche Diagnostics)). Samples were briefly sonicated and immunoprecipitated by incubating with anti-GFP agarose. The immunoprecipitates were washed extensively in lysis buffer, eluted in SDS sample buffer, and subjected to immunoblotting.

Senescence-associated beta-galactosidase (SA-βgal) assay

SA-βgal assay were performed based as previously described methods[41].

Measurement of telomere length

Genomic DNA was isolated from 1×10^6 cells. The telomere-specific oligonucleotide probe (5'-TTAGGGTTAGGGTTAGGGTTAGGG-3'; ValueGene) was end-labeled using γ-^{32}P-ATP (MP Biomedicals) and T4 polynucleotide kinase (NEB). Two μg of genomic DNA for each sample was digested with *Alu*I (NEB) and *Mbo*I (NEB) and subjected to Southern analysis with the telomere-specific probe. Mean telomere length was calculated from $\Sigma ODi/(\Sigma ODi/\Sigma MWi)$. ODi and MWi are optical density and molecular weight at a given position i, respectively.

Cell proliferation assay

Cell proliferation was determined with CellTiter 96® AQueous One Solution Cell Proliferation Assay (MTS (3-(4,5-Dimethylthiazol-2-yl)-2,5-diphenyltetrazolium)), according to the protocol provided by the manufacturer (Promega).

Statistical analysis

Results are presented as mean±s.d. Comparisons were performed with student's t-test or one-way anova. $p<0.05$ was defined as statistically significant.

Supplementary Material

Refer to Web version on PubMed Central for supplementary material.

Acknowledgements

We thank Lucio Comai for providing experimental material, Martin Hetzer, Jan Karlseder and Larry Gerace for helpful discussion, Mercè Marti for teratoma analysis, Meritxell Carrio Llach for karyotyping, Travis Berggren, Maggie Lutz, Ilir Dubova, Scott Stewart, Rupa Devi, and Jessica Kim for technical help, and May Schwarz for administrative help. GHL and LK were partially supported by a CIRM grant (TG2-01158), JQ was partially supported by an AFAR/Ellison Medical Foundation postdoctoral fellowship; ADP was partially supported by a NIH

training grant T32 CA009370. This study was supported by grants from NIH R01-DA025779 (KZ), and NIH P41 RR011823 (JY); the G. Harold and Leila Y. Mathers Charitable Foundation, Sanofi-Aventis, Ellison Medical Foundation, MICINN and Fundacion Cellex (JCIB).

References

1. Worman HJ, Ostlund C, Wang Y. Diseases of the nuclear envelope. Cold Spring Harb. Perspect. Biol. 2010; 2:a000760. [PubMed: 20182615]
2. Burtner CR, Kennedy BK. Progeria syndromes and ageing: what is the connection? Nat. Rev. Mol. Cell Biol. 2010; 11:567–578. [PubMed: 20651707]
3. Kudlow BA, Kennedy BK, Monnat RJ Jr. Werner and Hutchinson-Gilford progeria syndromes: mechanistic basis of human progeroid diseases. Nat. Rev. Mol. Cell Biol. 2007; 8:394–404. [PubMed: 17450177]
4. Merideth MA, et al. Phenotype and course of Hutchinson-Gilford progeria syndrome. N. Engl. J. Med. 2008; 358:592–604. [PubMed: 18256394]
5. Davies BS, Fong LG, Yang SH, Coffinier C, Young SG. The posttranslational processing of prelamin A and disease. Annu. Rev. Genomics Hum. Genet. 2009; 10:153–174. [PubMed: 19453251]
6. Olive M, et al. Cardiovascular Pathology in Hutchinson-Gilford Progeria: Correlation With the Vascular Pathology of Aging. Arterioscler. Thromb. Vasc. Biol. 2010
7. Ragnauth CD, et al. Prelamin A acts to accelerate smooth muscle cell senescence and is a novel biomarker of human vascular aging. Circulation. 2010; 121:2200–2210. [PubMed: 20458013]
8. Varga R, et al. Progressive vascular smooth muscle cell defects in a mouse model of Hutchinson-Gilford progeria syndrome. Proc. Natl. Acad. Sci. U. S. A. 2006; 103:3250–3255. [PubMed: 16492728]
9. Pegoraro G, et al. Ageing-related chromatin defects through loss of the NURD complex. Nat. Cell Biol. 2009; 11:1261–1267. [PubMed: 19734887]
10. Scaffidi P, Misteli T. Reversal of the cellular phenotype in the premature aging disease Hutchinson-Gilford progeria syndrome. Nat. Med. 2005; 11:440–445. [PubMed: 15750600]
11. Dechat T, et al. Nuclear lamins: major factors in the structural organization and function of the nucleus and chromatin. Genes Dev. 2008; 22:832–853. [PubMed: 18381888]
12. Scaffidi P, Misteli T. Lamin A-dependent nuclear defects in human aging. Science. 2006; 312:1059–1063. [PubMed: 16645051]
13. McClintock D, et al. The mutant form of lamin A that causes Hutchinson-Gilford progeria is a biomarker of cellular aging in human skin. PLoS. One. 2007; 2:e1269. [PubMed: 18060063]
14. Constantinescu D, Gray HL, Sammak PJ, Schatten GP, Csoka AB. Lamin A/C expression is a marker of mouse and human embryonic stem cell differentiation. Stem Cells. 2006; 24:177–185. [PubMed: 16179429]
15. Freberg CT, Dahl JA, Timoskainen S, Collas P. Epigenetic reprogramming of OCT4 and NANOG regulatory regions by embryonal carcinoma cell extract. Mol. Biol. Cell. 2007; 18:1543–1553. [PubMed: 17314394]
16. Peric-Hupkes D, et al. Molecular maps of the reorganization of genome-nuclear lamina interactions during differentiation. Mol. Cell. 2010; 38:603–613. [PubMed: 20513434]
17. Irizarry RA, et al. The human colon cancer methylome shows similar hypo- and hypermethylation at conserved tissue-specific CpG island shores. Nat. Genet. 2009; 41:178–186. [PubMed: 19151715]
18. Huang, d. W.; Sherman, BT.; Lempicki, RA. Systematic and integrative analysis of large gene lists using DAVID bioinformatics resources. Nat. Protoc. 2009; 4:44–57. [PubMed: 19131956]
19. Dennis G Jr. et al. DAVID: Database for Annotation, Visualization, and Integrated Discovery. Genome Biol. 2003; 4:3.
20. McClintock D, Gordon LB, Djabali K. Hutchinson-Gilford progeria mutant lamin A primarily targets human vascular cells as detected by an anti-Lamin A G608G antibody. Proc. Natl. Acad. Sci. U. S. A. 2006; 103:2154–2159. [PubMed: 16461887]

21. Gorenne I, Kavurma M, Scott S, Bennett M. Vascular smooth muscle cell senescence in atherosclerosis. Cardiovasc. Res. 2006; 72:9–17. [PubMed: 16824498]
22. Minamino T, Komuro I. Vascular cell senescence: contribution to atherosclerosis. Circ. Res. 2007; 100:15–26. [PubMed: 17204661]
23. Huang S, et al. Correction of cellular phenotypes of Hutchinson-Gilford Progeria cells by RNA interference. Hum. Genet. 2005; 118:444–450. [PubMed: 16208517]
24. Liu GH, et al. Regulation of myoblast differentiation by the nuclear envelope protein NET39. Mol. Cell Biol. 2009; 29:5800–5812. [PubMed: 19704009]
25. Washburn MP, Wolters D, Yates JR III. Large-scale analysis of the yeast proteome by multidimensional protein identification technology. Nat. Biotechnol. 2001; 19:242–247. [PubMed: 11231557]
26. Ruis BL, Fattah KR, Hendrickson EA. The catalytic subunit of DNA-dependent protein kinase regulates proliferation, telomere length, and genomic stability in human somatic cells. Mol. Cell Biol. 2008; 28:6182–6195. [PubMed: 18710952]
27. Li H, Vogel H, Holcomb VB, Gu Y, Hasty P. Deletion of Ku70, Ku80, or both causes early aging without substantially increased cancer. Mol. Cell Biol. 2007; 27:8205–8214. [PubMed: 17875923]
28. Espejel S, et al. Shorter telomeres, accelerated ageing and increased lymphoma in DNA-PKcs-deficient mice. EMBO Rep. 2004; 5:503–509. [PubMed: 15105825]
29. Han X, et al. Tethering by lamin A stabilizes and targets the ING1 tumour suppressor. Nat. Cell Biol. 2008; 10:1333–1340. [PubMed: 18836436]
30. Zhang J, et al. A human iPSC model of Hutchinson Gilford Progeria reveals vascular smooth muscle and mesenchymal stem cell defects. Cell Stem Cell. 2011; 8:31–45. [PubMed: 21185252]
31. Candelario J, Borrego S, Reddy S, Comai L. Accumulation of distinct prelamin A variants in human diploid fibroblasts differentially affects cell homeostasis. Exp. Cell Res. 2011; 317:319–329. [PubMed: 20974128]
32. Hockemeyer D, et al. A drug-inducible system for direct reprogramming of human somatic cells to pluripotency. Cell Stem Cell. 2008; 3:346–353. [PubMed: 18786421]
33. Vodyanik MA, Bork JA, Thomson JA, Slukvin II. Human embryonic stem cell-derived CD34+ cells: efficient production in the coculture with OP9 stromal cells and analysis of lymphohematopoietic potential. Blood. 2005; 105:617–626. [PubMed: 15374881]
34. Lu SJ, Ivanova Y, Feng Q, Luo C, Lanza R. Hemangioblasts from human embryonic stem cells generate multilayered blood vessels with functional smooth muscle cells. Regen. Med. 2009; 4:37–47. [PubMed: 19105615]
35. Kawamura T, et al. Linking the p53 tumour suppressor pathway to somatic cell reprogramming. Nature. 2009; 460:1140–1144. [PubMed: 19668186]
36. Deng J, et al. Targeted bisulfite sequencing reveals changes in DNA methylation associated with nuclear reprogramming. Nat. Biotechnol. 2009; 27:353–360. [PubMed: 19330000]
37. Bern M, Goldberg D, McDonald WH, Yates JR III. Automatic quality assessment of peptide tandem mass spectra. Bioinformatics. 2004; 20(Suppl 1):i49–i54. [PubMed: 15262780]
38. Eng J, McCormack A, Yates J. An Approach to Correlate Tandem Mass Spectral Data of Peptides with Amino Acid Sequences in a Protein Database. J Am Soc Mass Spectrom. 1994; 5:976–989. [PubMed: 24226387]
39. Peng J, Elias JE, Thoreen CC, Licklider LJ, Gygi SP. Evaluation of multidimensional chromatography coupled with tandem mass spectrometry (LC/LC-MS/MS) for large-scale protein analysis: the yeast proteome. J. Proteome. Res. 2003; 2:43–50. [PubMed: 12643542]
40. Sadygov RG, et al. Code developments to improve the efficiency of automated MS/MS spectra interpretation. J. Proteome. Res. 2002; 1:211–215. [PubMed: 12645897]
41. bacq-Chainiaux F, Erusalimsky JD, Campisi J, Toussaint O. Protocols to detect senescence-associated beta-galactosidase (SA-betagal) activity, a biomarker of senescent cells in culture and in vivo. Nat. Protoc. 2009; 4:1798–1806. [PubMed: 20010931]

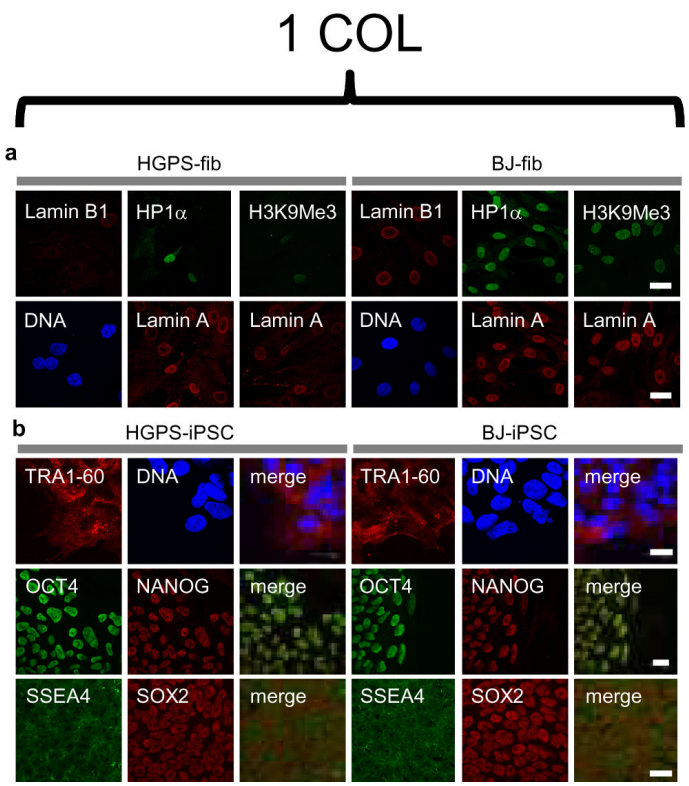

Figure 1. Generation and characterization of HGPS-iPSCs

a, Immunofluorescence analysis performed on HGPS (left) and BJ (right) fibroblasts at p17 with the indicated antibodies. **b**, Immunofluorescence analysis of the indicated pluripotent markers in HGPS-iPSCs (left) and BJ-iPSCs (right). Nuclei were visualized with Hoechst (blue). Scale bar, 20 μm.

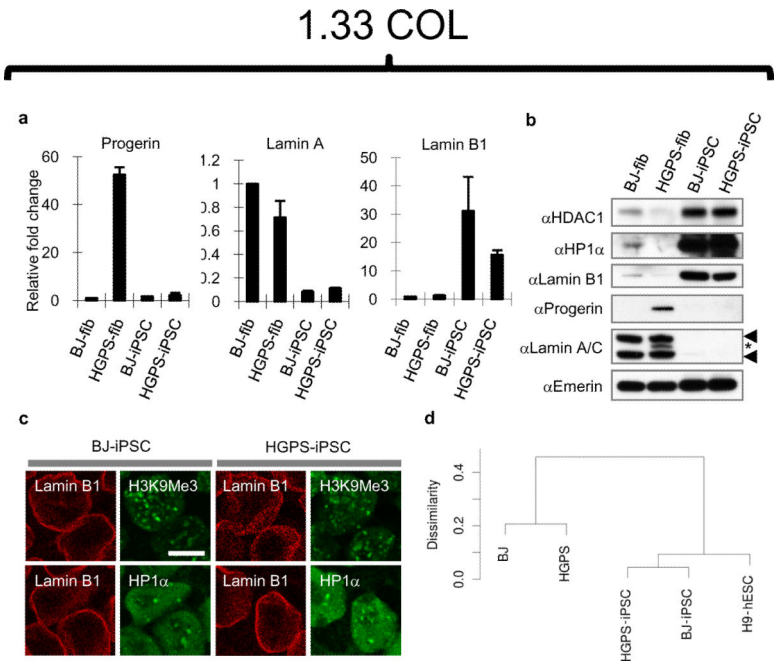

Figure 2. HGPS-associated nuclear defects are reset in HGPS-iPSCs

a, RT-PCR analysis of Progerin, Lamin A and Lamin B1 in the specific cell lines (n=3). **b**, Immunoblotting analysis of the indicated proteins. Emerin used as loading control. Asterisk denotes progerin (Δ50 lamin A). Arrowheads denote lamin A (upper) and lamin C (lower). **c**, Immunofluorescence analysis performed on BJ-iPSCs and HGPS-iPSCs for detection of the indicated proteins. Scale bar, 10 μm. **d**, Hierarchical clustering of genome-wide DNA methylation profiles.

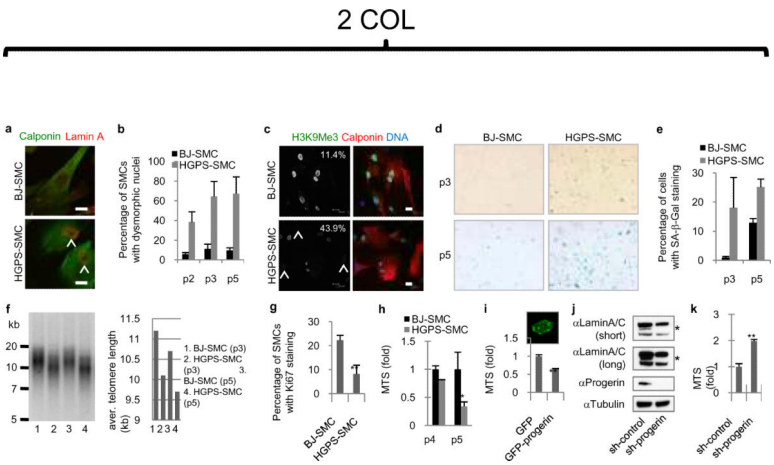

Figure 3. SMCs expressing progerin show nuclear defects and accelerated senescence

a, Immunostaining of calponin and lamin A in iPSC-derived SMCs (p5). Arrowheads denote dysmorphic nuclei. Scale bar, 20μm. **b**, Percentage of calponin-positive cells demonstrating dysmorphic nuclei, (n=3, $p<0.001$). **c**, Immunostaining of H3K9Me3 and calponin in iPSC-derived SMCs (p5). Nuclei were visualized with Hoechst (blue). Arrowheads denote decreased nuclear H3K9Me3 (percentage in corner). Scale bar, 20 μm. **d–e**, Senescence-associated (SA)-β-Gal staining of iPSC-derived SMCs, $p<0.05$. **f**, Southern blot analysis of SMCs showing telomere length (left). Quantified average of telomere length (right, n=2). **g**, Percentage of Ki67-positive cells in iPSC-derived SMCs (calponin-positive, p3), $^{**}p<0.01$. **h–i**, Cell proliferation analysis of iPSC-derived SMCs (n=3), $^{*}p<0.05$ (h) or primary vascular SMCs (overexpressing GFP or GFP-progerin, n=3), $^{**}p<0.01$ (i). Typical GFP-progerin-positive nucleus showing abnormal morphology (upper). **j**, Immunoblotting of the indicated proteins in shRNA-modified HGPS-iPSCs after 21 days of EB-mediated differentiation. Asterisks denote progerin (Δ50 laminA). **k**, Cell proliferation analysis of the SMCs derived from shRNA-modified HGPS-iPSCs (p2, n=3), $^{**}p<0.01$.

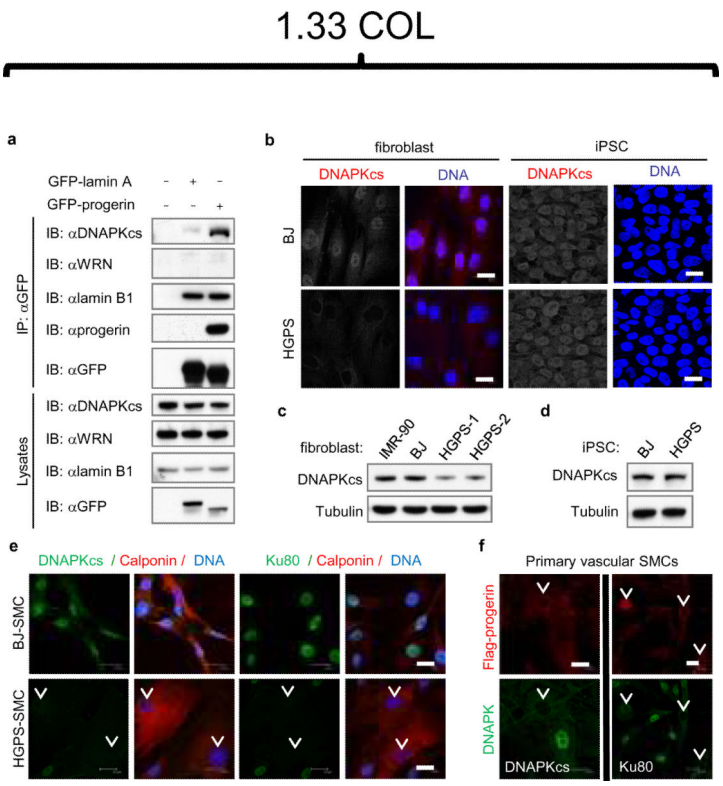

Figure 4. Decreased expression of DNAPK holoenzyme correlates with premature cell aging

a, Extracts from BJ fibroblasts expressing GFP, GFP-Lamin A, or GFP-Progerin, were immunoprecipitated with a GFP antibody and examined by immunoblotting analysis. **b**, DNAPKcs staining in the indicated cell lines. **c–d**, Immunoblot analysis of DNAPKcs expression. **e–f**, Immunostaining of the indicated proteins in iPSCs-derived SMCs (e) or primary vascular SMCs overexpressing progerin (f). Arrowheads denote decreased DNAPKcs or Ku80. Nuclei were visualized with Hoechst (blue). Scale bar, 20μm.